Structure, Vol. 12, 11–20, January, 2004, ©2004 Elsevier Science Ltd. All rights reserved. DOI 10.1016/j.str.2003.11.023

A Closed Binding Pocket and Global Destabilization Modify the Binding Properties of an Alternatively Spliced Form of the Second PDZ Domain of PTP-BL

Tine Walma,[1] Jan Aelen,[1] Sander B. Nabuurs,[1,2] Marlies Oostendorp,[1] Lieke van den Berk,[3] Wiljan Hendriks,[3] and Geerten W. Vuister[1,*]
[1]Department of Biophysical Chemistry
NSRIM Center
University of Nijmegen
Toernooiveld 1
6525 ED Nijmegen
[2]Center for Molecular and Biomolecular Informatics
University of Nijmegen
Toernooiveld 1
P.O. Box 9010
6500 GL Nijmegen
[3]Department of Cell Biology
Institute of Cellular Signaling
University of Nijmegen
Geert Grooteplein 28
6525 GA, Nijmegen
The Netherlands

Summary

PTP-BL is a large phosphatase that is implicated in cellular processes as diverse as cytokinesis, actin-cytoskeletal rearrangement, and apoptosis. Five PDZ domains mediate its cellular role by binding to the C termini of target proteins, forming multiprotein complexes. The second PDZ domain (PDZ2) binds to the C termini of the tumor suppressor protein APC and the LIM domain-containing protein RIL; however, in one splice variant, PDZ2as, a 5 residue insertion abrogates this binding. The insert causes distinct structural and dynamical changes in the alternatively spliced PDZ2: enlarging the L1 loop between β2 and β3, both lengthening and changing the orientation of the α2 helix, giving the base of the binding pocket less flexibility to accommodate ligands, and destabilizing the entire domain. These changes render the binding pocket incapable of binding C termini, possibly having implications in the functional role of PTP-BL.

Introduction

PTP-BL is a large cytosolic protein which contains a N-terminal domain with multiple potential phosphorylation sites, a FERM domain, common to membrane-cytoskeleton linker proteins, five PDZ domains (labeled PDZ1–PDZ5), and a C-terminal phosphatase domain. The FERM domain is responsible for localization to the membrane side of epithelial cells (Cuppen et al., 1999b) and can be cosedimented with filamentous actin (Herrmann et al., 2003). Studies showed that overexpression of catalytically inactive PTP-BL in HeLa cells led to defects in cytokinesis and resulted in multinucleate cells (Herrmann et al., 2003), but the underlying substrates have not yet been identified. To date, PTP-BL has been found capable of dephosphorylating the proteins RIL (Cuppen et al., 1998), β-catenin (Erdmann et al., 2000), Src, and ephrin B (Palmer et al., 2002). However, most attempts at elucidating the biological role of PTP-BL have been focused on identifying binding partners for its five PDZ domains, protein modules that bind to C termini and orchestrate the formation of multiprotein complexes (van Ham and Hendriks, 2003).

The PDZ domains of PTP-BL have been shown to interact with several proteins: PDZ1 interacts with BP75 (Cuppen et al., 1999a), both PDZ2 and PDZ4 with TRIP6 and RIL (Cuppen et al., 1998, 2000), PDZ2 interacts with APC (Erdmann et al., 2000) and RA-GEF-2 (Kozlov et al., 2002), PDZ3 binds to PRK2 (Gross et al., 2001), and PDZ4 binds to ephrin B1 (Palmer et al., 2002) and CRIP2 (van Ham et al., 2003). It is clear from these many studies that the PDZ domains of PTP-BL can interact with multiple proteins; however, the functional implications of these interactions have yet to be linked in a coherent scheme. A reported binding of the PDZ2 domain of PTP-BAS (the human ortholog of PTP-BL, also known as PTPL1, FAP-1, PTP1e, and PTPN13) to the human Fas receptor led to a proposed role in apoptosis regulation (Sato et al., 1995), but this finding was subsequently challenged by other studies (Cuppen et al., 1997; Walma et al., 2002). The interactions with RIL, TRIP6, and CRIP2 all reveal actin-cytoskeleton-related staining patterns and the interactions with PARG, a Rho-specific GTPase-activating protein (Saras et al., 1997), and PRK2, a Rho effector kinase (Gross et al., 2001) support a role for PTP-BL in microfilament dynamics. In addition, PTP-BL has been linked to actin-cytoskeletal rearrangements induced by ephrinB ligand signaling (Palmer et al., 2002). Although its precise function is unknown, mutations in APC have been linked to human familial and sporadic colon cancer (Erdmann et al., 2000). Finally, overexpression studies in HeLa cells suggest a role for PTP-BL in the regulation of cytokinesis (Herrmann et al., 2003).

The web of intracellular interactions involving PTP-BL is further complicated by its four isoforms. These isoforms result from alternative splicing and have specific expression patterns (Maekawa et al., 1999; Saras et al., 1994; Banville et al., 1994; Erdmann et al., 2000; Herrmann et al., 2003). The four isoforms result from splice differences in three different regions. The first alternatively spliced region corresponds to the central part of the N-terminal domain. This domain was shown to be responsible for midbody localization during cytokinesis (Herrmann et al., 2003). The second region encodes the protein region between the FERM domain and PDZ1. The third region involves residues within the PDZ2 domain. Due to alternative splice donor sites, either a short PDZ2 domain of 93 residues or an alternatively spliced isoform containing 98 residues is produced (Erdmann et al., 2000). The difference of 5 residues between the shorter PDZ2 domain and its longer splice variant in isoform 4 (PDZ2as) has been reported to effectively abrogate binding to the C termi-

*Correspondence: vuister@nmr.kun.nl

nus of APC (Erdmann et al., 2000). Isoform 4 was also shown to be involved in the regulation of cytokinesis and cosedimented with microtubules (Herrmann et al., 2003).

The distribution and ratio of the two PDZ2 splice forms show that PDZ2as-containing mRNA transcripts are coexpressed with PDZ2-containing transcripts in most tissue and cell types (Sato et al., 1995; Erdmann et al., 2000). The deduced tissue expression pattern of PDZ2as ranges from virtually absent (kidney) to ~20% of PTP-BL mRNAs (lung). Thus, the ratio is cell-type specific. Since both the protein stability and subcellular distribution could differ for the two PDZ2 splice variants, it may well be that local ratios at specific subcellular sites differ from the above estimates.

The interactions of PDZ domains with C termini are generally grouped into four classes. Class I interactions involve S/Txϕ* sequences (where ϕ is a hydrophobic amino acid and * is the terminal carboxyl tail), class II involves ϕxϕ* C termini, class III, E/Dxϕ*, and class IV, VxD/E sequences (Vaccaro and Dente, 2002). It is well documented that PDZ domains are promiscuous, able to bind C termini across classes. For example, the Erbin PDZ domain can bind both class I and II C termini (Birrane et al., 2003), while PDZ2 from PTP-BL is able to bind both class I and III C termini (Walma et al., 2002). It remains to be determined whether this adaptability of PDZ domains is related to their function as protein adaptors.

PDZ domains are globular domains containing two α helices and six β strands. The binding pocket is located between the α2 helix and β2 strand. C-terminal ligands are bound by several conserved interactions (Vaccaro and Dente, 2002), such as specific hydrogen bonding to the β2 strand, insertion of the P^0 (ultimate C-terminal) residue into a hydrophobic pocket, and various interactions involving the P^{-2} (antepenultimate) residue, depending on the interaction class. Other residues of ligands may also contribute, and residues up to P^{-7} have been shown to interact with PDZ domains (Birrane et al., 2003). Exceptions to the general structural motif for PDZ domain-mediated interactions are known to exist. For example, PDZ7 from GRIP contains a closed, canonical binding pocket which is thought to be unable to classically bind peptides and instead interacts with the C terminus of GRASP-1 via a hydrophobic patch on its β4-β5-α2 face (Feng et al., 2002).

The structure of the short PDZ2 domain from PTP-BL was previously solved by us (Walma et al., 2002). Here, we report the structure of the alternatively spliced PDZ2 domain from PTP-BL (PDZ2as), corresponding to isoform 4. This insert strikingly abrogates the interaction with class I and III ligands derived from the tumor suppressor protein APC and the LIM domain-containing protein RIL. Our results show that pronounced structural and dynamical changes render PDZ2as incapable of binding C termini.

Results

Using high-resolution NMR, we determined an ensemble of 30 structures of the alternatively spliced PDZ2 domain of mouse PTP-BL (Figure 1A). PDZ2as possesses a well-structured PDZ fold. The pairwise backbone RMS deviation for the ordered regions is 0.60 ± 0.11 Å (Table 1). Figure 1C shows a structural superposition of PDZ2 (Walma et al., 2002) with PDZ2as. Both domains possess similar β sheet and α-helical elements. Four of the inserted residues extend the L1 loop, while the initial valine structurally replaces a glycine in PDZ2, becoming the last residue in the β2 strand. Unlike PDZ2, the L1 loop extends unrestricted into space. In addition, the α2 helix of PDZ2as is orientated differently. In PDZ2, β2 and α2 are virtually parallel, but in PDZ2as, the orientation of the α2 helix angle has changed by ~20° (Figure 1D), remodeling the binding pocket (vide infra).

Figure 1E shows the sequence alignment of PDZ2as with its own shorter PDZ2 variant, as well as with several representative PDZ domains. The secondary structural elements of these domains are well conserved. The different binding preference of the PDZ domain from CASK for class II peptides (Vaccaro and Dente, 2002) is reflected by structural differences in the α2 helices. The alignment also shows that the structure of PDZ7 from GRIP is the most divergent structure from PDZ2as, with wide regions of the two domains being dissimilar. These differences also correlate with its altered binding properties.

To investigate the precise differences in the size and shape of the binding pockets of PDZ2 and PDZ2as, we compared their sizes and volumes using the program CASTp (Liang et al., 1998). CASTp probes pockets and cavities in protein structures and characterizes these using solvent accessible areas and volumes. We analyzed the binding pockets of PDZ2, PDZ2as, and PDZ7 (GRIP). To obtain an insight into the inherent variation of PDZ domains, we compared these results to the averages obtained from five PDZ crystal structures. The results of this analysis are listed in Table 2. The mouth of the binding pocket in PDZ2 has an area of 105 ± 46 $Å^2$ and a volume of 55 ± 40 $Å^3$. These values decrease significantly to 64 ± 24 $Å^2$ and 23 ± 17 $Å^3$ in PDZ2as. The pocket mouth area and volume of the X-ray structures are comparable to those of PDZ2, in both magnitude and variability. In contrast, GRIP displays values more comparable to those of PDZ2as. These results correlate with the binding pocket widths between the β2 strand and the α2 helix. The PDZ domains with smaller binding pockets are narrower at their base, averaging below 6 Å, while those with larger pockets are wider, averaging above 6.5 Å. Thus, like the GRIP domain, PDZ2as has a constricted binding pocket, with both a smaller mouth and much less volume to accommodate ligands.

To further understand the effects of the splice insert on the structure of the PDZ2as domain, we determined its amide exchange characteristics. The exchange rate is slow in regions that are protected from the solvent, such as the protein core, and fast in regions that are exposed. The data can also be interpreted to yield information about the overall stability (Huyghues-Despointes et al., 1999). The results are displayed in Figure 1B. The core of the PDZ2as domain is formed by several highly protected residues in the β1, β3, β4, and β6 strands. These residues correlate with cross-strand hydrogen

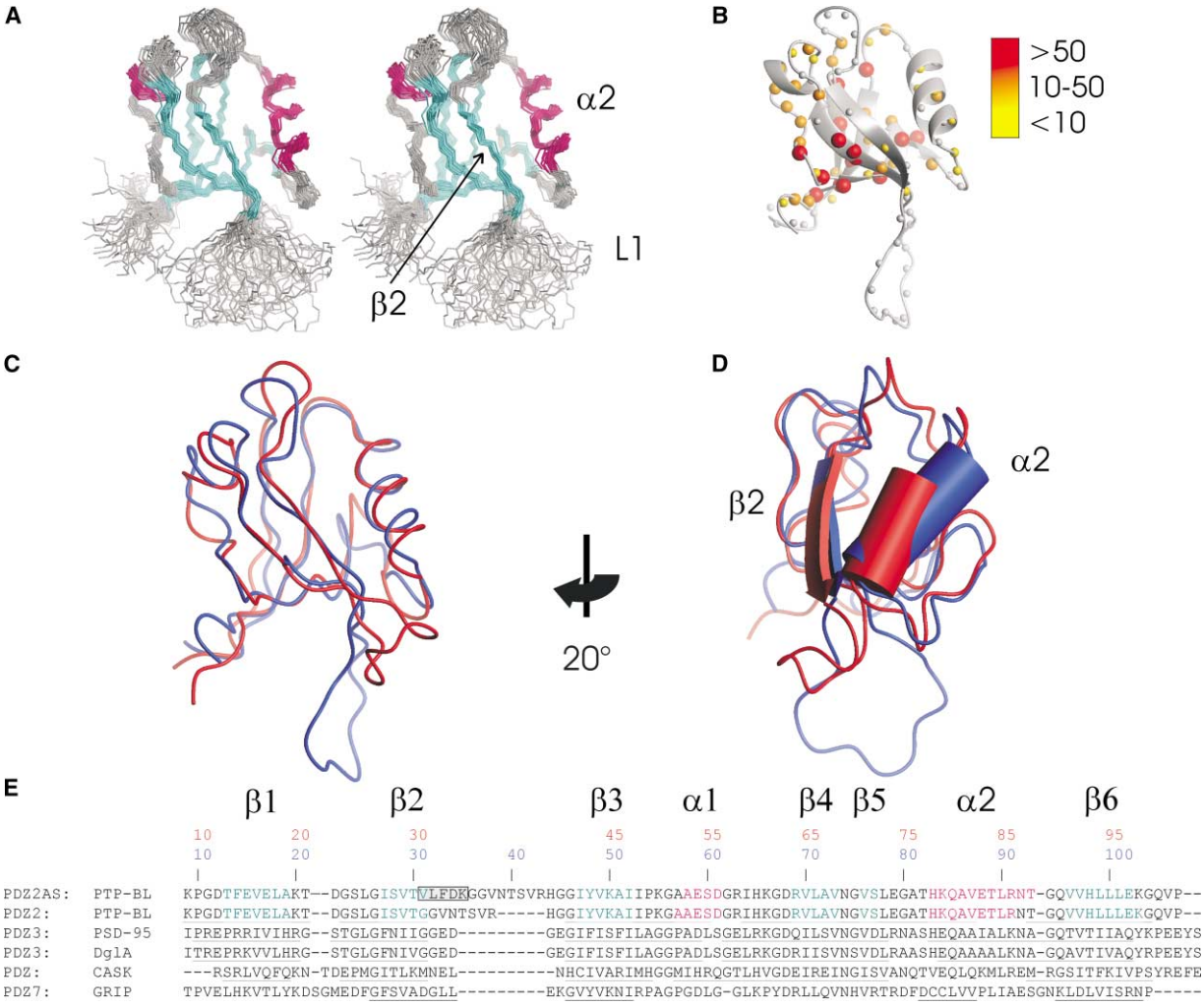

Figure 1. Structural Ensemble and Sequence Alignment of PD22as

(A) Structural ensemble of PDZ2as (stereo diagram); secondary structures are indicated by cyan (β strand) and pink (α helix).

(B) Protection of amides from H/D exchange. Amides are depicted as spheres; red spheres indicate amides with high protection factors, orange spheres, those with intermediate protection factors, and yellow spheres represent amide with low protection factors. Gray spheres indicate amides with complete solvent exchange within the experimental dead time of 20 min.

(C and D) Structural superposition of PDZ2as (blue) with PDZ2 (red). The orientation of the α2 helices differ by ~20° (shown as cylinders) while that of the β2 strands remain the same (shown as arrows).

(E) PDZ2as (PDB code 1ozi) sequentially aligned with GRIP (1m5z), CASK (1kwa), PSD-95 (1bfe), and DglA (1pdr). The alignments were performed on each domain with a maximal displacement of 7 Å for each pair of C^{α} atoms and a global RMS limit of 4 Å. Protein regions that are structurally similar to PDZ2as are indicated by underlining. Secondary structures of both PDZ2 and PDZ2as complexes are colored as in (A). The 5 residue insertion is boxed in gray. Numbering schemes are given for PDZ2as (blue) and, for reference, PDZ2 (red).

bonding interactions. In contrast, amides in the loops, termini, and binding pocket are almost freely exchangeable, most exchanging faster than the 20 min experimental dead time. Noticeably, amides in the binding pocket have low or unmeasurable protection factors, indicating full solvent accessibility.

Because the low levels of amide protection show that this domain is very flexible, we decided to investigate in detail how the mobility of this domain contributes to its altered binding characteristics. We determined the $\{^1H\}^{15}N$-NOE, ^{15}N-R_1, and ^{15}N-$R_{1\rho}$ relaxation rates (Figure 2) for the PDZ2as domain and compared these to the results obtained for the PDZ2 domain. We calculated the order parameters (S^2), internal correlation times (τ_e), and chemical exchange contributions (R_{ex}) for each residue. The global tumbling rate τ_c of 6.12 ns is a typical value for a protein of this size. Most of the secondary structural elements for PDZ2as display S^2 values above the 0.82 average. Loop L1 is much more flexible than the rest of the protein, with low $\{^1H\}^{15}N$-NOE values that translate into low S^2 values and moderate τ_e contributions.

In addition to the L1 loop, several other residues show significant flexibility. Leu25 is located in the "GLGF loop" preceding the β2 strand. The flexibility of Val106 indicates the end of the domain. The flexibility of Arg91 and Gly94 appear to be linked. This type of concerted flexibility, also observed in the shorter PDZ2 domain,

Table 1. Structural Statistics for the Alternatively Spliced PDZ2 Domain of PTP-BL (PDZ2as)

Structural Statistics	PDZ2as
Restraint Information	
Distance restraints	1354
(Intraresidual/sequential/medium/long)	(554/311/128/361)
Hydrogen bonding restraints	29
Dihedral angle restraints (phi)	76
Average rms deviation from experimental restraints	
Distance restraints (Å)	0.032 ± 0.001
Dihedral angle restraints (°)	0.230 ± 0.204
Pairwise Cartesian rms deviation (Å)	
Global backbone heavy atoms	1.28 ± 0.14
Global all heavy atoms	3.22 ± 0.58
Ordered[a] backbone heavy atoms	0.60 ± 0.11
Ordered[a] all heavy atoms	2.60 ± 0.73
Ramachandran quality parameters (%)[b]	
Residues in favored regions	79.1
Residues in allowed regions	17.0
Residues in additionally allowed regions	2.2
Residues in disallowed regions	1.7
Average rms deviation from current reliable structures (rms Z scores, null deviation = 1)[b]	
Bond lengths	1.040
Bond angles	1.129
Omega angle restraints	1.361
Side chain planarity	1.155
Improper dihedral distribution	0.824
Inside/outside distribution	0.989
Average deviation from current reliable structures (Z scores, null deviation = 0)[b]	
Second generation packing quality	−2.048
Ramachandran plot appearance	−3.278
Chi-1/chi-2 rotamer normality	−1.598
Backbone conformation	−2.434

[a] Residues involved in secondary structure: 13–19, 27–31, 47–53, 58–61, 68–73, 76–77, 83–93, and 96–103.
[b] Values based on WHAT-CHECK reports, which are available for every structure deposited in the Protein Data Bank.

involved the preceding residues of Leu90 and Thr93. The conformation of this region differs in the two ensembles; in PDZ2as these residues favor a 3_{10} helical conformation, while in PDZ2 they form a turn-like structure. These conformational differences lead to altered hydrogen bonding patterns. For instance, in PDZ2as, the side chain oxygen of Thr93 hydrogen bonds to both the carboxyl of Leu90 and the amide of Gly94, while in PDZ2, this side chain of Thr93 hydrogen bonds only to the carboxyl of Leu90.

We compared the PDZ2 and PDZ2as domains using the program QUEEN (Nabuurs et al., 2003) (*qu*antitative *e*valuation of *e*xperimental *N*MR restraints). QUEEN allows users to quantify and rank NOEs by how much structural information each contributes to a structure. Table 3 lists the 25 most important NOEs in PDZ2. It is interesting that Val29 is involved in 5/25 of these structurally important NOEs. The single most important NOE between Val29 and Leu90 anchors the β2 strand to the α2 helix across the binding pocket. This NOE is clearly present in the PDZ2 spectra, and it is just as clearly absent in PDZ2as spectra. In the PDZ2as ensemble this distance is 1.5 Å longer than in PDZ2, placing it beyond typical NOESY detection limits (Wuthrich, 1986). The NOE between the side chain methyl groups of Val16 and Gly62 is also not observed in the PDZ2as spectra. Gly62 is located in the irregular α1-to-β4 turn region, which differs structurally in the two ensembles. In PDZ2, several hydrophobic contacts between Val33 and the β5-to-α2 turn structure the L1 loop. However, in PDZ2as, these contacts involve Val31. The insertion additionally disrupts other NOEs that constrain the loop in PDZ2. Other than the aforementioned exceptions, we were able to locate the balance of the NOEs listed in Table 3 in the respective NOESY spectra.

We further validated the structural differences between PDZ2 and PDZ2as using residual dipolar couplings. We measured $^1D_{HN}$ RDCs for both domains and calculated Q factors. Q factors represent the agreement between structurally predicted and experimentally measured dipolar couplings; lower values indicate better agreement (Cornilescu et al., 1998). The RDCs for the PDZ2as domain, although not used in the structure refinement, show very good agreement with its structure, with a Q factor of 0.23. The PDZ2 domain also agrees well with own RDCs with a Q factor of 0.36. However, these dipolar coupling data sets are not interchangeable. For instance, when the $^1D_{NH}$ RDC data set from PDZ2 is superposed onto PDZ2as structure, the Q factor rises to 0.52, reflecting an essential structural rearrangement of the PDZ2as structure with respect to PDZ2. These results are illustrated in Figure 3C. The predicted and measured RDCs of PDZ2as show good agreement, whereas the dipolar couplings of the PDZ2 domain superposed on the PDZ2as structure are skewed, with several outliers greater than 10 Hz.

We tested the binding properties of PDZ2as using two peptides to represent the class I and III C termini that are known to interact with PDZ2. One peptide was derived from APC (Erdmann et al., 2000) and the second

Table 2. Solvent Accessible Mouth Area, Pocket Volume, and Surface Area of the Wall Atoms of the Binding Pocket

PDZ Domain	Protein	Mouth Area (Å^2)	Pocket Volume (Å^3)	Area of Wall Atoms of Binding Pocket (Å^2)	Width of Base of Binding Pocket (Å)
PDZ2[a]	PTP-BL	105 ± 46	55 ± 40	24 ± 20	6.5 ± 1.1
PDZ2as [a]	PTP-BL	64 ± 24	23 ± 17	11 ± 7	5.8 ± 0.9
PDZ[b]	X-ray	125 ± 36	89 ± 16	36 ± 5	7.5 ± 1.4
PDZ7 [a]	GRIP	40 ± 19	12 ± 10	6 ± 5	5.6 ± 0.6

The binding pocket widths are calculated from the Cα-Cα distance between residues that structurally align with Thr30 and His83 in PDZ2as. Error bars are 1σ.
[a] The values represent the average of values obtained for the 11 conformers with lowest pairwise rms deviation.
[b] The values represent the average obtained for five uncomplexed PDZ domain structures solved by X-ray diffraction, taken from PDB accession codes 1kwa, 1g9o, 1gq4, 1gq5, and 1n99.

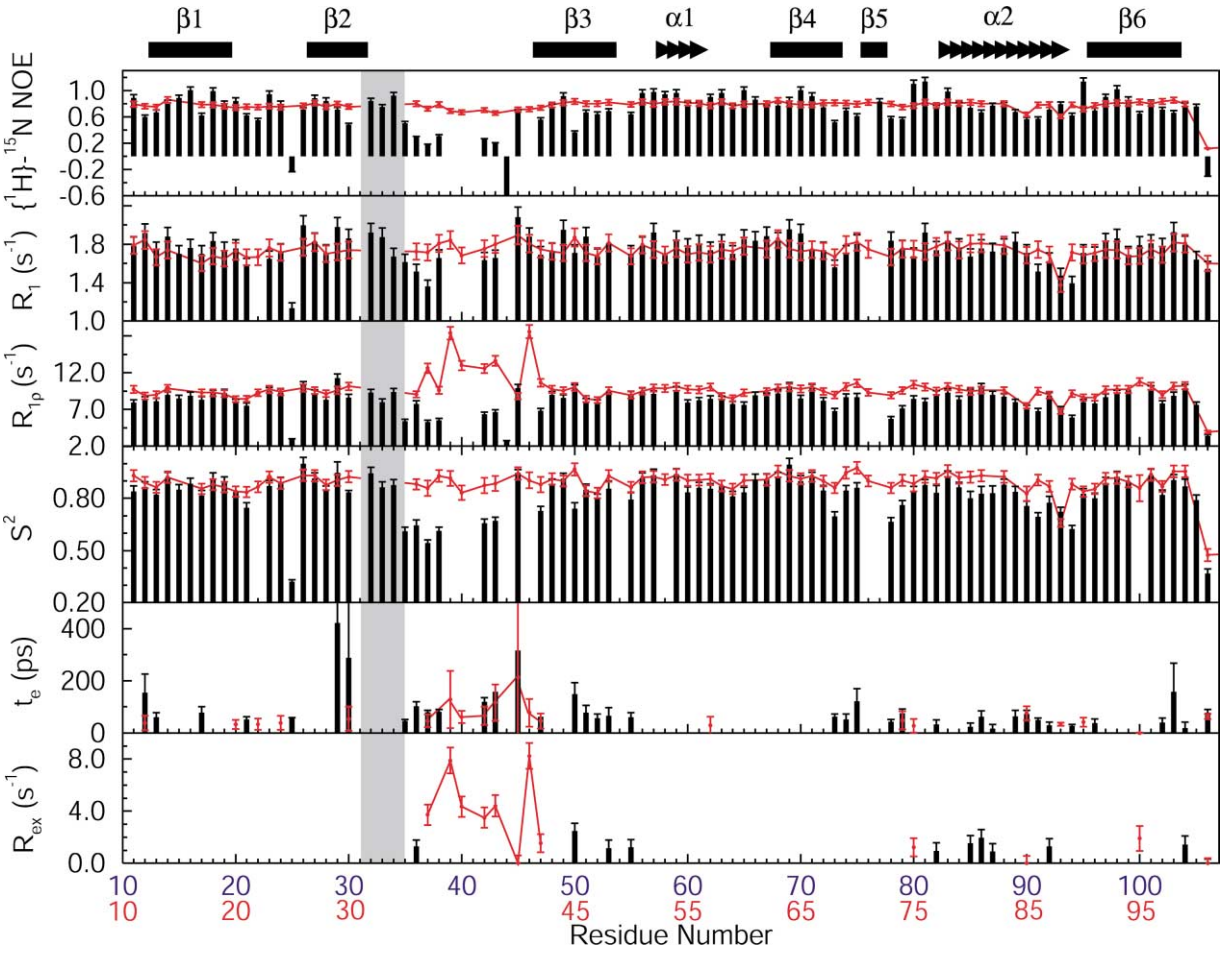

Figure 2. Dynamics of PDZ2as Compared with PDZ2

The experimental relaxation data ({^{1}H}^{15}N-NOE, R_1 and $R_{1\rho}$) were fit to yield values for S^2, τ_e, and R_{ex} for PDZ2as (black bars) and PDZ2 (Walma et al., 2002) (red line) as a function of residue number. Numbering refers to PDZ2as (blue) and PDZ2 (red). The secondary structure of PDZ2as is indicated at the top, helices (triangles) and strands (bars). The 5 residue insertion is shaded gray.

was derived from RIL (Walma et al., 2002). We were especially interested in the binding properties of APC because it was previously reported that the tight binding of APC with PDZ2 was completely abolished with PDZ2as (Erdmann et al., 2000). Figures 3A and 3B clearly demonstrate the difference in binding affinities of these two domains. For PDZ2as, the amide of Gly26 is marginally affected by the presence of the ligand, while it shifts more than 0.5 ppm in case of the PDZ2 domain. These two ligands bind to PDZ2 with varying affinities; the K_d of APC was previously reported to be as strong as 8.1 nM based on SPR measurements (Erdmann et al., 2000), whereas our own NMR data show this interaction to be in the intermediate exchange regime with a K_d of 200 μM (Figure 3B). The interaction of PDZ2 with the RIL peptide was determined by NMR to be in the fast exchange regime (often associated with weak interactions) with a K_d of 1.1 mM (Walma et al., 2002).

Both the APC and RIL C-terminal ligands bind very poorly to PDZ2as with interactions in the fast exchange regime. In fact, only 3 residues show signs of interaction with the APC ligand, with minor chemical shift changes. However, it is interesting to note that two of these residues are located in the binding pocket of PDZ2as (i.e., Gly26 and Ile27). Due to the weakness of the interaction, a dissociation constant for the APC ligand could not be determined. The effects of the RIL/PDZ2as interaction were also small, but clearly present. Approximately half of the residues showed perceptible interactions; in particular Gly26 shifted more than 60 Hz (0.1 ppm). Based on these data, we determined the K_d of the RIL ligand to be ~19 mM.

Discussion

Structure and Flexibility

The PDZ2as ensemble is well defined with very good local geometry, as indicated by the low Q factor of 0.23 for the $^1D_{NH}$ RDCs. Some regions of the domain are unique to PDZ2as, such as the long L1 loop connecting the β2 and β3 strands. The flexibility of the loop is clearly demonstrated by the relaxation data, with order parameters ranging from 0.6 to 0.7 and also by low amide protection factors. Unexpectedly, the inserted residues Leu32, Phe33, and Asp34 have S^2 values of ~0.9, which are typical of secondary structural elements, while the

Table 3. Comparison of Distances Corresponding to the 25 Most Structurally Important NOEs in the PDZ2 and PDZ2as Ensembles

Rank	Residue 1		Residue 2		PDZ2 (Å)	PDZ2as (Å)	Difference (Å)
1	***Val***	***29 $(H^{\gamma1})_3/(H^{\gamma2})_3$***	***Leu***	***90 H^N***	***6.8 ± 0.7***	***8.3 ± 1.2***	***+1.5***
2	Leu	25 $(H^{\delta1})_3/(H^{\delta2})_3$	Val	97 H^β	4.1 ± 1.2	3.8 ± 1.8	−0.3
3	Val	73 $(H^{\gamma1})_3/(H^{\gamma2})_3$	Ala	86 H^α	5.4 ± 0.6	6.2 ± 2.1	+0.8
4	**Val**	**29 $(H^{\gamma1})_3/(H^{\gamma2})_3$**	**Val**	**49 H^α**	**4.7 ± 0.7**	**4.8 ± 1.2**	**+0.1**
5	*Val*	*16 $(H^{\gamma1})_3/(H^{\gamma2})_3$*	*Gly*	*62 H^N*	*6.9 ± 0.6*	*9.0 ± 1.1*	*+2.1*
6	Ile	64 $(H^{\delta1})_3$	Leu	101 $(H^{\delta1})_3/(H^{\delta2})_3$	5.1 ± 1.3	4.3 ± 1.3	−0.9
7	**Val**	**29 $(H^{\gamma1})_3/(H^{\gamma2})_3$**	**Ala**	**86 $H^{\beta2}$/ $H^{\beta3}$**	**5.1 ± 1.8**	**4.6 ± 1.6**	**−0.5**
8	Ile	47 H^β	Leu	78 $(H^{\delta1})_3/(H^{\delta2})_3$	4.7 ± 2.3	4.9 ± 1.2	+0.3
9	**Val**	**29 $(H^{\gamma1})_3/(H^{\gamma2})_3$**	**Val**	**87 H^α**	**5.0 ± 0.8**	**5.7 ± 2.1**	**+0.7**
10	Leu	101 $H^{\delta1}$/ $H^{\delta2}$	Lys	103 H^N	5.8 ± 0.9	7.7 ± 1.0	+1.9
11	Ile	47 $(H^{\gamma2})_3$	Val	70 H^β	3.5 ± 0.8	3.7 ± 1.4	+0.3
12	Lys	20 $H^{\epsilon2}/H^{\epsilon3}$	Val	97 $(H^{\gamma2})_3/(H^{\gamma3})_3$	5.2 ± 2.7	5.2 ± 2.1	0.0
13	Arg	69 H^N	Val	106 H^N	3.6 ± 2.2	6.4 ± 2.4	+2.8
14	Arg	69 H^N	Glu	102 $H^{\beta2}/H^{\beta3}$	4.0 ± 0.8	4.8 ± 1.6	+0.7
15	Val	70 H^α	Leu	101 H^α	2.9 ± 1.0	2.5 ± 0.4	−0.4
16	Pro	10 $H^{\beta2}$/ $H^{\beta3}$	Gln	105 H^α	3.3 ± 2.3	6.6 ± 3.4	+3.2
17	Val	97 $(H^{\gamma1})_3/(H^{\gamma2})_3$	Leu	99 H^N	5.6 ± 0.5	5.3 ± 1.0	−0.3
18	*Val*	*38 H^N*	*Thr*	*82 H^α*	*2.5 ± 0.6*	—	*+Large*
19	Val	16 $(H^{\gamma1})_3/(H^{\gamma2})_3$	Leu	99 H^γ	4.4 ± 0.9	7.6 ± 0.8	+3.2
20	*Asn*	*39 H^N*	*Thr*	*82 H^α*	*3.9 ± 2.1*	—	*+Large*
21	*Val*	*42 $(H^{\gamma1})_3/(H^{\gamma2})_3$*	*Ile*	*47 H^α*	*6.4 ± 1.9*	—	*+Large*
22	**Val**	**29 $(H^{\gamma1})_3/(H^{\gamma2})_3$**	**Val**	**87 H^N**	**6.1 ± 1.3**	**5.9 ± 2.5**	**−0.2**
23	Ile	47 $(H^{\gamma2})_3$	Val	87 H^N	6.3 ± 0.2	6.4 ± 1.3	0.0
24	Val	16 H^N	Gly	99 H^N	3.3 ± 0.5	3.5 ± 0.3	+0.2
25	Ile	47 H^β	Val	70 H^β	2.8 ± 1.5	2.0 ± 0.2	−0.7

Structurally important NOEs were determined using the program QUEEN. NOEs involving Val29 are shown in bold and NOEs not observed in the PDZ2as structure are italicized. Distances involving methyl groups refer to a $1/r^{-6}$ averaging, resulting from nonstereospecific assignments.

rest of the L1 loop is much more flexible when compared to PDZ2.

The pattern of amide protection factors indicates that the core of the protein is located on the opposite side of the PDZ domain to the binding pocket. The amides of loops and turns were freely exchangeable within the experimental dead time. The binding pocket is also very unprotected, even the α2 helix, which is surprising because α helices typically have high protection factors due to their regular hydrogen bonding patterns.

The conformational stability, ΔG_{HX}, calculated from the three amides with the highest protection factors reveals a low thermodynamic stability of 2.8 kcal/mol for PDZ2as (Huyghues-Despointes et al., 1999). Indeed, the amide exchange rates could only be determined at low pH and temperature. This value is much lower than the 4.8 ± 0.4 kcal/mol stabilization which was reported for the short human ortholog of PDZ2 (Ekiel et al., 1998), and is also lower than the 3.2 and 4.8 kcal/mol stabilities reported for the first and second PDZ domains of syntenin (Kang et al., 2003). The relatively fast exchange of even the most protected amides indicates that they are transiently solvent exposed because of the intrinsic flexibility. There is a noticeable difference in mobility between the ordered and loop regions in PDZ2as, while in PDZ2 this difference is negligible (Figure 2). Thus, in PDZ2as, the insertion appears to cause a global destabilization which affects the loop and turn regions even more than the ordered regions. This destabilization is also suggested by the substantially decreased lifetime of the domain in the NMR tube, reduced from more 2 years for PDZ2 to a period of weeks for PDZ2as.

Other residues in or near the binding pocket also show significant flexibility. The linked flexibility of Arg91 and Gly94 appears to be inherent since this type of linkage was also observed in PDZ2 between residues Leu90 and Thr93. We explained this linkage as resulting from a hydrogen bond between the side chain oxygen of Thr93 and the H^N of Leu90 (Walma et al., 2002). In both PDZ2 and PDZ2as, this linked flexibility retains its position relative to the end of the C-terminal helix cap of α2, since this helix is longer in PDZ2as. We hypothesize that this linked flexibility is involved structurally in C-terminal capping; however, we have not excluded the possibility that the mobility of these residues has a functional role.

Interactions

The APC and RIL ligands bind to the PDZ2 domain of PTP-BL with dissociation constants of 200 μM and 1.1 mM (Walma et al., 2002). The dissociation constants for the interactions of these two peptides with PDZ2as are reduced to levels that are not physiologically relevant, i.e., undeterminable and ~19 mM for APC and RIL, respectively, in accordance with prior biochemical and SPR data.

Dissociation constants for other PDZ-ligand complexes serve as useful comparisons. The K_d of a class I peptide interaction with the human ortholog of PDZ2, confirmed by Gdm-HCl denaturation and fluorescence emission spectroscopy, was reported to be in the 30 μM range (Ekiel et al., 1998). Studies on the PDZ domains of syntenin using ITC and fluorescence have yielded K_d values in the low- to midmicromolar range (Kang et al., 2003). These dissociation constants are consistent with the function of PDZ domains as protein adaptors: high enough to attract binding partners yet still weak enough to allow the binding partner to disengage after other biologically important interactions have taken place.

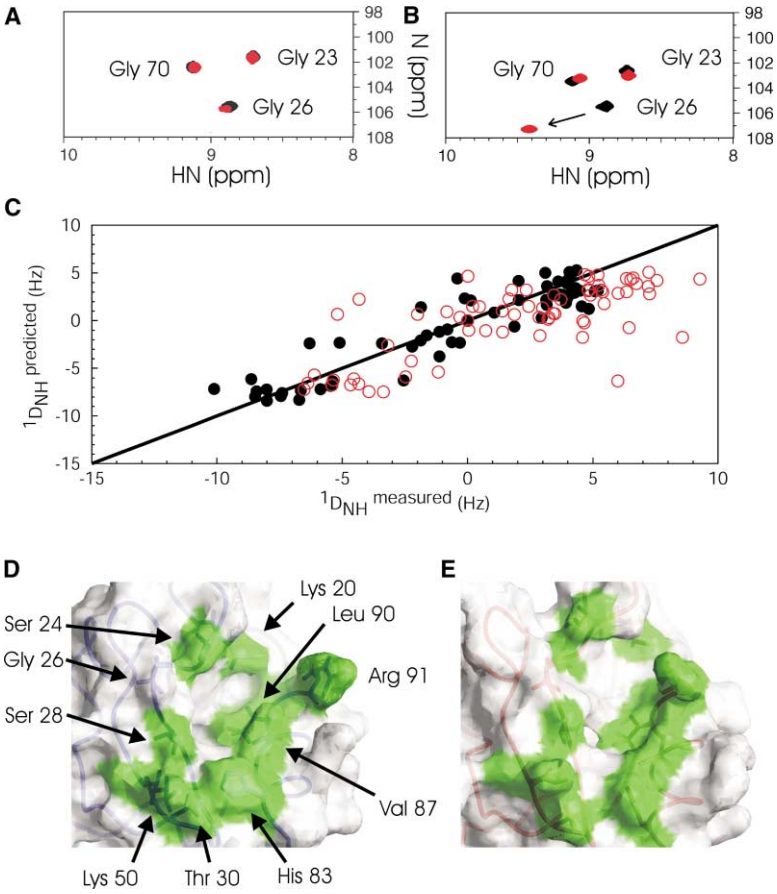

Figure 3. Ligand Binding and Structural Changes in PDZ2as

(A and B) Excerpts of ^{15}N-HSQC spectra from PDZ2as and PDZ2. Superposed are the spectra of each domain alone (black) and in complex with the APC ligand (red). The C terminus of APC interacts minimally with PDZ2as (A) but strongly with PDZ2 (B).

(C) Measured versus predicted $^1D_{NH}$ RDCs. Black data points show the $^1D_{HN}$ RDCs of PDZ2as fitted to its own ensemble (Q factor 0.23). Red circles show the $^1D_{HN}$ RDC of PDZ2 fitted onto the PDZ2as ensemble (Q factor 0.52).

(D and E) Comparison of the binding pocket size and shape of PDZ2as (D) with that of PDZ2 (E). The size and mouth area of the binding pocket of PDZ2as is smaller than that of PDZ2. Residues that form the binding pocket mouth are surface colored in green. The backbones of PDZ2as and PDZ2 are traced in blue and red respectively.

It is interesting to note that the C-terminal ligands still preferentially interact with PDZ2as in the binding pocket, as evinced by chemical shift changes for a key binding site residue Gly26 (Figures 3A and 3B); however, it appears that the increased sterical hindrance prevents efficient binding. Furthermore, the class III RIL sequence retains more interaction ability with PDZ2as than the class I APC sequence. A reason for this could be that the longer P^{-2} glutamic acid side chain of the RIL ligand is more able to maintain its interaction with the His83 side chain, thus conserving more of the interactions that are necessary for binding (Novak et al., 2002).

To find out why ligand binding in PDZ2as is abolished, we completed a detailed structural comparison of PDZ2 and PDZ2as. The binding pocket of PDZ2as is substantially shorter, shallower, and narrower than that of PDZ2, with a 2.4 times smaller volume, a 1.5 times smaller mouth size, and a 0.7 Å narrower base (Table 2). In particular, several side chains now extend into the binding pocket, markedly affecting the conformation (Figure 3D). This obstruction can be explained by the differing α2 helix positions. In PDZ2, β2 and α2 are mostly parallel, while in PDZ2as, their angles differ by $\sim$20° (Figure 1D). This causes the N-terminal end of the α2 helix to rise and the C-terminal end to drop. These changes result in a narrower pocket (Table 2). It is possible that the smaller binding pocket of PDZ2as retains an altered specificity for ligands that are able to avoid the problems introduced by the increased steric hindrance, such as ligands containing residues with smaller side chains.

Because the insert is in very close proximity to the reactive site histidine (His83), we were concerned that its protonation state would be affected, preventing the proper interaction with the bound ligand. Thus, we assigned the side chains of all the histidines in PDZ2 and PDZ2as. From the resulting chemical shift data we concluded that all the histidine residues in the two domains remain unaffected by the insertion and remain in the $N^{\epsilon 2}$ singly protonated state (data not shown).

Structural Effects of Insertions

The insertion actively disrupts the contacts in the L1 loop, unanchoring it from the β5-to-α2 turn, and removing several important hydrophobic contacts that structured the L1 loop in PDZ2. The relaxation data and amide exchange rates clearly show that both the β5-to-α2 turn and the L1 loop are more flexible, supporting this unanchoring hypothesis. The new hydrophobic contacts between β2 strand (in particular Val31) and the β5-to-α2 turn rigidify the base of the binding pocket by replacing one of the two glycine-glycine hinges that flanked the L1 loop in PDZ2 with a Val/Leu sequence. This hinge was postulated to give the loop an overall slow dynamic motion, as the large R_{ex} values in the L1 loop of PDZ2 suggest (Figure 2). This particular section of the L1 loop in PDZ2as is restrained, the S^2 value of Leu32 is $\sim$0.1 higher than that of the structurally equivalent glycine in PDZ2. In addition, the amides of two inserted residues (30 and 32) are more protected than the rest of the β2

strand with measurable protection factors of 6 and 5.8, also indicating that this region of the protein is less exposed. We postulate that the displacement of this mobile glycine hinge and the introduction of new hydrophobic contacts contribute to the abrogation of binding, altering the flexibility of the base of the binding pocket and making it less able to accommodate ligands. The altered angle of the α2 helix also disrupts key contacts across the binding pocket, notably between two structurally important residues, Val29 and Leu90.

Insertions and deletions in proteins are most easily accommodated in loops, turns, and coils because these regions are the most structurally accommodative, exposed to solvent and flexible (Pascarella and Argos, 1992). Therefore, it is not unexpected that the extra residues in PDZ2as form part of an extended L1 loop. Other studies have also examined the structural and functional roles of loops in proteins. These studies show that loop insertions or deletions typically result in minor adjustments to the overall protein structure, indicating the propensity of proteins to maintain the favorable interactions essential to their tertiary structures (Ramasubbu et al., 2003; Banerjee et al., 1998; Mossing, 1998). In addition, these studies show that the protein counterpart with the longer loop tends to be more unstable than the one with a shorter loop, regardless of which one constitutes the wild-type (Ramasubbu et al., 2003; Banerjee et al., 1998; Mossing, 1998). For example, it was found that insertions in T4 lysozyme destabilized the protein from 1 to 6 kcal/mol (Vetter et al., 1996).

Similar stability results have been acquired for other PDZ domains. The first PDZ domain of syntenin contains a 4 residue longer β2-to-β3 loop in comparison to its second PDZ domain and this correlates with a lower domain stabilization (3.2 versus 4.8 kcal/mol), higher overall flexibility, a narrower peptide binding pocket (1.8 Å narrower at the base), and lower affinities for identical ligands (Kang et al., 2003). Likewise, the extension of the L1 loop in PDZ2as has decreased the overall stability of the domain and significantly altered the binding pocket conformation and ligand binding abilities. However, this is the first reported instance that intradomain splicing has been shown to affect the binding properties of a PDZ domain.

Most interestingly, the insert affects the PDZ2 binding properties "from a distance"; it is not necessary for the five inserted residues in the splice variant to physically obstruct the binding pocket to significantly impair this domain's ligand binding abilities. Rather, the replacement of the Gly-Gly hinge with the more conformationally restricted Val-Leu sequence appears to be critical. The insertion results in a higher global flexibility, and the adjustment of the hydrophobic core ultimately results in altered binding pocket conformation and binding properties. Thus, the alternative PDZ2 splice variant provides nature with an ingenious method to modulate the functional properties of this domain and the current data give a structural and dynamical explanation of these functional differences.

Experimental Procedures

Sample Preparation

A RT-PCR was performed on mouse lung RNA using the SMART PCR cDNA synthesis kit (Clontech), and the cDNA products were used as template for a PCR with PDZ2-specific primers. These products were then cloned into the pGEM-T vector (Promega). The presence of the 5 residue insertion was determined by sequencing. Finally, the PDZ2as domain was cloned into a pGEX-2T (Pharmacia) plasmid. Protein expression was induced at 37°C under ampicillin selection in *Escherichia coli* BL21 Codon Plu (DE3) RIL competent cells (Stratagene) by the addition of 0.2 mM IPTG for 2.5 hr. Uniformly $^{15}N/^{13}C$-labeled PDZ2 samples were prepared using 1 g/l of ^{15}N NH_4Cl and 3 g/l ^{13}C glucose as sole nitrogen and carbon sources. The cell pellet was resuspended in 1× PBS buffer (pH 7.7) in the presence of 1 mM aprotinin, 1 mM PMSF and Complete protease inhibitor, sonificated, and then centrifuged twice at 10,000 rpm at 4°C for 30 min to remove cell debris. The supernatant was bound to glutathione agarose beads (Molecular Probes) and washed with 1× PBS buffer. Elution from the column was performed by 15 mM reduced glutathione at pH 7.7. To cleave the GST tag, 10 U/ml thrombin protease was added in three incubations at room temperature, for 18, 5, and finally for 24 hr. This mixture of protein was concentrated by first dialyzing against water for 24 hr at 4°C, lyophilizing, and finally redissolving in 1× PBS buffer. The resulting mixture was then passed over a Sephadex G75 size exclusion column at room temperature and then appropriate fractions were collected, dialyzed once more against water overnight, lyophilized, and stored at −75°C. NMR samples contained ~1.4 mM dissolved protein in a buffer of 50 mM KH_2PO_4/K_2HPO_4 and 50 mM KCl, pH 6.8, H_2O/D_2O (95%/5%), using traces of Complete protease inhibitor and NaN_3 as preservatives. The H/D amide exchange rate experiments were recorded at 8.5°C using a 1.1 mM sample dissolved in a pH 3.5 D_2O buffer (50 mM acetate/50 mM KCl). The isotropic samples for measuring $^1D_{HN}$ residual dipolar couplings contained 0.5 mM $^{13}C/^{15}N$-labeled protein at pH 9 while aligned samples contained an additional 10 mg/ml filamentous Pf1 phage (Asla Labs). The coordinates of the PDZ2as ensemble were deposited in the Protein Data Bank under PDB code 1ozi, and the chemical shifts, ^{15}N relaxation, amide exchange, and RDC data were deposited in the BioMagResBank under BMRB accession number 5762.

Peptide Interactions

The RIL C-terminal peptide contained an N-terminal biotin group and a C-terminal carboxyl group. The peptide sequences correspond to the final twelve C-terminal residues of RIL and the APC C-terminal peptide corresponds to the final 10 residues (accession numbers NP_062290 and NP_031488). The peptides were titrated to more than 3.2 equivalents into individual 1 mM ^{15}N-labeled protein samples. The differences in backbone H^N and N chemical shifts were monitored with ^{15}N-HSQC spectra recorded at 600 MHz and 25°C. The vectors of the (initial − final) H^N and N frequencies (Hz) versus the relative concentrations were fit using a least-squares procedure to determine dissociation constants for the peptides.

NMR Spectroscopy

NMR experiments were collected at 25°C on a double-labeled $^{13}C/^{15}N$ sample with the exception of the ^{15}N NOESY-HSQC, which was recorded on a ^{15}N sample. The NMR experiments were carried out on Varian Unity Inova 600 and 800 MHz spectrometers. All data were processed and analyzed using the NMRPipe (Delaglio et al., 1995) suite and XEASY (Bartels et al., 1995). Resonance assignments were completed using 3D HNCA, HNHA, HNCACB, and (H)CCH-TOCSY experiments. The side chains of the histidine residues were assigned by first correlating the C^β frequency with $C^{\delta 2}/H^{\delta 3}$ and, second, correlating the $C^{\delta 2}/H^{\delta 2}$ with $N^{\epsilon 2}$, and $N^{\epsilon 2}$ with $C^{\epsilon 1}/H^{\epsilon 1}$ using constant time/sensitivity enhanced experiments. The distance restraints were obtained from an aliphatic 3D ^{13}C NOESY-HSQC recorded on a Varian 800 MHz and a 3D ^{15}N NOESY-HSQC (sensitivity enhanced) recorded on a Varian 600 MHz, each with mixing times of 100 ms. $^3J(H^NH^\alpha)$-coupling constants were derived from a 3D HNHA experiment. ^1H-^{15}N residual dipolar couplings were recorded using the IPAP-type sensitivity enhanced ^{15}N-HSQC experiments. Peaks were reassigned using HNCA experiments. Structurally predicted RDCs were calculated using the program MODULE v1.0 (Dosset et al., 2001). Amide exchange rates were determined by recording sensitivity enhanced ^{15}N-HSQC spectra of the pH 3.5 sample at 8.5°C over 144 hr. The rate constants for H/D amide exchange were obtained

from the peak intensity decay and time data (starting from solvation in D_2O buffer). The data was nonlinearly least-squares fit to a single exponential function using the program modelXY (Delaglio et al., 1995). Protection factors were also calculated, $PF = k_{int}/k_{obs}$, where k_{int} is the intrinsic exchange rate of a residue at a particular pH and temperature. The intrinsic rate constants were determined using the program Sphere (Zhang, 1995; Bai et al., 1993). The relaxation experiments T_1, $T_{1\rho}$, and $\{^1H\}^{15}N$-NOE were recorded at 25°C at 14.1 T (600 MHz). The relaxation delays for the T_1 experiments were T = 0.0160, 0.3840, 0.5120, 0.6400, 1.0240 s. The relaxation delays for the $T_{1\rho}$ experiment were T = 0.0160, 0.0320, 0.0480, 0.0960, 0.1120, 0.1280 s. The relaxation data were fit using the program Modelfree 4.0 (Mandel et al., 1995). We determined the isotropic model accurately describes the PDZ2as data by fitting the $R_1/R_{1\rho}$ of the core residues using the program TENSOR (Dosset et al., 2000).

Structure Refinement

The NOE peak volumes were converted into distance ranges by normalization against peak volumes that were calibrated to known distances, and then overestimated 2-fold. Distance restraint ranges were defined with lower limits of the van der Waals radii and upper limits of 2.8, 3.5, 5.0, or 7.0 Å. 76 phi angle restraints were obtained from ^3J (H^NH^α) couplings. Hydrogen bonding restraints were derived from characteristic NOE patterns and H/D amide exchange data. The H^N-O and the N-O hydrogen bonding distances were restrained from 1.2 to 2.2 Å and 2.2 to 3.2 Å, respectively. An initial set of 200 NMR structures was calculated using a Cartesian-space simulated annealing protocol in X-PLOR version 3.851 (Brunger, 1996). This resulted in a set of 73 structures with no distance restraint violations >0.5 Å and no dihedral angle violations $>5°$. To improve local geometry and electrostatics, these 73 structures were then refined in water using a restrained molecular dynamics protocol under a CHARMM22 force field (MacKerell et al., 1998; Spronk et al., 2002). Of these, the 30 lowest energy structures were selected to form the final ensemble. Structures were analyzed using the programs PROCHECK-NMR (Laskowski et al., 1996), WHAT-IF (Vriend, 1990), and QUEEN (Nabuurs et al., 2003), and compared to the $^1D_{HN}$ residual dipolar couplings.

Received: May 19, 2003
Revised: September 9, 2003
Accepted: September 26, 2003
Published: January 13, 2004

References

Bai, Y., Milne, J.S., Mayne, L., and Englander, S.W. (1993). Primary structure effects on peptide group hydrogen exchange. Proteins *17*, 75–86.

Banerjee, S., Pieper, U., Kapadia, G., Pannell, L.K., and Herzberg, O. (1998). Role of the omega-loop in the activity, substrate specificity, and structure of class A beta-lactamase. Biochemistry *37*, 3286–3296.

Banville, D., Ahmad, S., Stocco, R., and Shen, S.H. (1994). A novel protein-tyrosine phosphatase with homology to both the cytoskeletal proteins of the band 4.1 family and junction-associated guanylate kinases. J. Biol. Chem. *269*, 22320–22327.

Bartels, C.H., Xia, T.-H., Billeter, M., Güntert, P., and Wüthrich, K. (1995). The program XEASY for computer-supported NMR spectral analysis of biological macromolecules. J. Biomol. NMR *6*, 1–10.

Birrane, G., Chung, J., and Ladias, J.A. (2003). Novel mode of ligand recognition by the Erbin PDZ domain. J. Biol. Chem. *278*, 1399–1402.

Brunger, A.T. (1996). X-PLOR Version 3.851. A System for X-Ray Crystalography and NMR (New Haven, CT: Yale University Press).

Cornilescu, G., Marquardt, J.L., Ottiger, M., and Bax, A. (1998). Validation of protein structure from anisotropic carbonyl chemical shifts in a dilute liquid crystalline phase. J. Am. Chem. Soc. *120*, 6836–6837.

Cuppen, E., Nagata, S., Wieringa, B., and Hendriks, W. (1997). No evidence for involvement of mouse protein-tyrosine phosphatase-BAS-like Fas-associated phosphatase-1 in Fas-mediated apoptosis. J. Biol. Chem. *272*, 30215–30220.

Cuppen, E., Gerrits, H., Pepers, B., Wieringa, B., and Hendriks, W. (1998). PDZ motifs in PTP-BL and RIL bind to internal protein segments in the LIM domain protein RIL. Mol. Biol. Cell *9*, 671–683.

Cuppen, E., van Ham, M., Pepers, B., Wieringa, B., and Hendriks, W. (1999a). Identification and molecular characterization of BP75, a novel bromodomain-containing protein. FEBS Lett. *459*, 291–298.

Cuppen, E., Wijers, M., Schepens, J., Fransen, J., Wieringa, B., and Hendriks, W. (1999b). A FERM domain governs apical confinement of PTP-BL in epithelial cells. J. Cell Sci. *112*, 3299–3308.

Cuppen, E., van Ham, M., Wansink, D.G., de Leeuw, A., Wieringa, B., and Hendriks, W. (2000). The zyxin-related protein TRIP6 interacts with PDZ motifs in the adaptor protein RIL and the protein tyrosine phosphatase PTP-BL. Eur. J. Cell Biol. *79*, 283–293.

Delaglio, F., Grzesiek, S., Vuister, G.W., Zhu, G., Pfeifer, J., and Bax, A. (1995). NMRPipe: a multidimensional spectral processing system based on UNIX pipes. J. Biomol. NMR *6*, 277–293.

Dosset, P., Hus, J.C., Blackledge, M., and Marion, D. (2000). Efficient analysis of macromolecular rotational diffusion from heteronuclear relaxation data. J. Biomol. NMR *16*, 23–28.

Dosset, P., Hus, J.C., Marion, D., and Blackledge, M. (2001). A novel interactive tool for rigid-body modeling of multi-domain macromolecules using residual dipolar couplings. J. Biomol. NMR *20*, 223–231.

Ekiel, I., Banville, D., Shen, S.H., and Gehring, K. (1998). Effect of peptide binding on amide proton exchange rates in the PDZ2 domain from human phosphatase hPTP1E. Biochem. Cell Biol. *76*, 334–340.

Erdmann, K.S., Kuhlmann, J., Lessmann, V., Herrmann, L., Eulenburg, V., Muller, O., and Heumann, R. (2000). The Adenomatous Polyposis Coli-protein (APC) interacts with the protein tyrosine phosphatase PTP-BL via an alternatively spliced PDZ domain. Oncogene *19*, 3894–3901.

Feng, W., Fan, J.S., Jiang, M., Shi, Y.W., and Zhang, M. (2002). PDZ7 of glutamate receptor interacting protein binds to its target via a novel hydrophobic surface area. J. Biol. Chem. *277*, 41140–41146.

Gross, C., Heumann, R., and Erdmann, K.S. (2001). The protein kinase C-related kinase PRK2 interacts with the protein tyrosine phosphatase PTP-BL via a novel PDZ domain binding motif. FEBS Lett. *496*, 101–104.

Herrmann, L., Dittmar, T., and Erdmann, K.S. (2003). The protein tyrosine phosphatase PTP-BL associates with the midbody and is involved in the regulation of cytokinesis. Mol. Biol. Cell *14*, 230–240.

Huyghues-Despointes, B.M., Scholtz, J.M., and Pace, C.N. (1999). Protein conformational stabilities can be determined from hydrogen exchange rates. Nat. Struct. Biol. *6*, 910–912.

Kang, B.S., Cooper, D.R., Jelen, F., Devedjiev, Y., Derewenda, U., Dauter, Z., Otlewski, J., and Derewenda, Z.S. (2003). PDZ tandem of human syntenin. Crystal structure and functional properties. Structure *11*, 459–468.

Kozlov, G., Banville, D., Gehring, K., and Ekiel, I. (2002). Solution structure of the PDZ2 domain from cytosolic human phosphatase hPTP1E complexed with a peptide reveals contribution of the beta2-beta3 loop to PDZ domain-ligand interactions. J. Mol. Biol. *320*, 813–820.

Laskowski, R.A., Rullmann, J.A., MacArthur, M.W., Kaptein, R., and Thornton, J.M. (1996). AQUA and PROCHECK-NMR: programs for checking the quality of protein structures solved by NMR. J. Biomol. NMR *8*, 477–486.

Liang, J., Edelsbrunner, H., and Woodward, C. (1998). Anatomy of protein pockets and cavities: measurement of binding site geometry and implications for ligand design. Protein Sci. *7*, 1884–1897.

MacKerell, A.D., Bashford, D., Bellott, M., Dunbrack, R.L., Evanseck, J.D., Field, M.J., Fischer, S., Gao, J., Guo, H., Ha, S., et al. (1998). All-atom empirical potential for molecular modeling and dynamics studies of proteins. J. Phys. Chem. B *102*, 3586–3616.

Maekawa, K., Imagawa, N., Naito, A., Harada, S., Yoshie, O., and Takagi, S. (1999). Association of protein-tyrosine phosphatase PTP-BAS with the transcription-factor-inhibitory protein IkappaBalpha

through interaction between the PDZ1 domain and ankyrin repeats. Biochem. J. *337*, 179–184.

Mandel, A.M., Akke, M., and Palmer, A.G. (1995). Backbone dynamics of Escherichia coli ribonuclease HI: correlations with structure and function in an active enzyme. J. Mol. Biol. *246*, 144–163.

Mossing, M.C. (1998). Solution structure and dynamics of a designed monomeric variant of the lambda Cro repressor. Protein Sci. *7*, 983–993.

Nabuurs, S.B., Spronk, C.A.E.M., Krieger, E., Maassen, H., Vriend, G., and Vuister, G.W. (2003). Quantitative evaluation of experimental NMR restraints. J. Am. Chem. Soc. *125*, 12026–12034.

Novak, K.A., Fujii, N., and Guy, R.K. (2002). Investigation of the PDZ domain ligand binding site using chemically modified peptides. Bioorg. Med. Chem. Lett. *12*, 2471–2474.

Palmer, A., Zimmer, M., Erdmann, K.S., Eulenburg, V., Porthin, A., Heumann, R., Deutsch, U., and Klein, R. (2002). EphrinB phosphorylation and reverse signaling: regulation by Src kinases and PTP-BL phosphatase. Mol. Cell *9*, 725–737.

Pascarella, S., and Argos, P. (1992). Analysis of insertions/deletions in protein structures. J. Mol. Biol. *224*, 461–471.

Ramasubbu, N., Ragunath, C., and Mishra, P.J. (2003). Probing the role of a mobile loop in substrate binding and enzyme activity of human salivary amylase. J. Mol. Biol. *325*, 1061–1076.

Saras, J., Claesson-Welsh, L., Heldin, C.H., and Gonez, L.J. (1994). Cloning and characterization of PTPL1, a protein tyrosine phosphatase with similarities to cytoskeletal-associated proteins. J. Biol. Chem. *269*, 24082–24089.

Saras, J., Franzen, P., Aspenstrom, P., Hellman, U., Gonez, L.J., and Heldin, C.H. (1997). A novel GTPase-activating protein for Rho interacts with a PDZ domain of the protein-tyrosine phosphatase PTPL1. J. Biol. Chem. *272*, 24333–24338.

Sato, T., Irie, S., Kitada, S., and Reed, J.C. (1995). FAP-1: a protein tyrosine phosphatase that associates with Fas. Science *268*, 411–415.

Spronk, C.A., Linge, J.P., Hilbers, C.W., and Vuister, G.W. (2002). Improving the quality of protein structures determined by NMR spectroscopy. J. Biomol. NMR *22*, 281–289.

Vaccaro, P., and Dente, L. (2002). PDZ domains: troubles in classification. FEBS Lett. *512*, 345–349.

van Ham, M., and Hendriks, W. (2003). PDZ domains - glue and guide. Mol. Biol. Rep. *30*, 69–82.

van Ham, M., Croes, H., Schepens, J., Fransen, J., Wieringa, B., and Hendriks, W. (2003). Cloning and characterization of mCRIP2, a mouse LIM-only protein that interacts with PDZ domain IV of PTP-BL. Genomics *8*, 631–644.

Vetter, I.R., Baase, W.A., Heinz, D.W., Xiong, J.P., Snow, S., and Matthews, B.W. (1996). Protein structural plasticity exemplified by insertion and deletion mutants in T4 lysozyme. Protein Sci. *5*, 2399–2415.

Vriend, G. (1990). WHAT IF: a molecular modeling and drug design program. J. Mol. Graph. *8*, 52–56, 29.

Walma, T., Spronk, C.A., Tessari, M., Aelen, J., Schepens, J., Hendriks, W., and Vuister, G.W. (2002). Structure, dynamics and binding characteristics of the second PDZ domain of PTP-BL. J. Mol. Biol. *316*, 1101–1110.

Wuthrich, K. (1986). NMR of Proteins and Nucleic Acids (New York: Wiley-Interscience).

Zhang, Y. (1995). Protein and Peptide Structure and Interactions Studied by Hydrogen Exchange and NMR. (Philadelphia, PA: University of Pennsylvania).

Accession Numbers

The coordinates of the PDZ2as ensemble were deposited in the Protein Data Bank under PDB code 1ozi, and the chemical shifts, ^{15}N relaxation, amide exchange, and RDC data were deposited in the BioMagResBank under BMRB accession number 5762.

Note Added in Proof

Similar results have been reported independently: N. Kachel et al. (2003), J. Mol. Biol. *334*, 143–155.